Hydrogen bonding in metalloporphyrins. Mechanistic study of the reactions of (tetraphenylporphinato)iron(III) azide with imidazole and N-methylimidazole

ARTICLE *in* INORGANIC CHEMISTRY · DECEMBER 1986

Impact Factor: 4.76 · DOI: 10.1021/ic00246a036

9 AUTHORS, INCLUDING:

William Byers
Ulster University
15 PUBLICATIONS **471** CITATIONS
SEE PROFILE

Ashfaq Mahmood
Chiba University
52 PUBLICATIONS **910** CITATIONS
SEE PROFILE

Contribution from the Departments of Chemistry, University of Ulster, Coleraine, Northern Ireland BT52 1SA, and Brown University, Providence, Rhode Island 02912

Hydrogen Bonding in Metalloporphyrins. Mechanistic Study of the Reactions of (Tetraphenylporphinato)iron(III) Azide with Imidazole and *N*-Methylimidazole

W. Byers,† J. A. Cossham,† J. O. Edwards,‡ A. T. Gordon,† J. G. Jones,*† E. T. P. Kenny,† A. Mahmood,‡ J. McKnight,† D. A. Sweigart,*‡ G. A. Tondreau,‡ and T. Wright†

Received July 11, 1986

The reaction of $Fe(TPP)N_3$ with imidazole (HIm) and *N*-methylimidazole (MeIm) has been studied in acetone and dichloromethane. Kinetic measurements at room temperature as well as low-temperature spectroscopic, conductivity, and electrochemical studies were used to fully characterize the intermediate complex $Fe(TPP)(RIm)N_3$ as six-coordinate and low spin. This complex reacts further to give $Fe(TPP)(RIm)_2^+N_3^-$. The rate-limiting step in the overall reaction is azide ionization from $Fe(TPP)(RIm)N_3$ to give the high-spin $Fe(TPP)(RIm)^+N_3^-$. The activation free energy of this step is ca. 3 kcal lower with HIm compared to that with MeIm because of hydrogen bonding to the departing azide ion in the transition state; this acceleration via hydrogen bonding is an entropic effect. A detailed comparison of M(Por)X systems is presented for M = Fe and Co, Por = TPP, PPIX, and PPIXDME, and X = F^-, Cl^-, Br^-, and N_3^-. The importance of spin changes on the kinetics and thermodynamics of intermediate and product formation is quantified. Hydrogen-bonding effects are found to have a greater influence on the kinetics than on the thermodynamics. The spin change for the reaction $Fe(TPP)(RIm)N_3 \rightarrow Fe(TPP)(RIm)^+N_3^-$ is $S = {}^1/_2 \rightarrow {}^5/_2$, and this is manifested in loss of CFSE (large ΔH^*) and a ΔS^* about 15 cal deg^{-1} mol^{-1} more positive than those found for analogous metalloporphyrin reactions that do not feature a spin change.

Introduction

Ferric porphyrin chlorides and fluorides are known[1-9] to react with imidazole type bases (RIm) as shown in eq 1. Undoubtedly this reaction proceeds stepwise according to eq 2 and 3, but

$$Fe(Por)X + 2RIm \overset{\beta_2}{\rightleftharpoons} Fe(Por)(RIm)_2^+X^- \quad (1)$$

$$Fe(Por)X + RIm \overset{K_1}{\rightleftharpoons} Fe(Por)(RIm)X \quad (2)$$

$$Fe(Por)(RIm)X + RIm \overset{K_2}{\rightleftharpoons} Fe(Por)(RIm)_2^+X^- \quad (3)$$

generally the intermediate species Fe(Por)(RIm)X is not observed because the formation constant for the addition of the second RIm (K_2) is larger than that for the first addition (K_1). While thermodynamics requires that the equilibrium concentration of Fe(Por)(RIm)X in solution be insignificant, kinetic studies[10-14] have demonstrated that its transient concentration can be large, especially at low temperatures. The Fe(Por)(RIm)X complexes are dynamically unstable with respect to X^- displacement and typically have a half-life of ca. 0.1 s at room temperature. Nevertheless, we[10-15] have thoroughly characterized them by using a variety of techniques (kinetics, conductivity, ESR, low-temperature optical spectroscopy, and cyclic voltammetry) and shown that the Fe(Por)(RIm)Cl and Fe(Por)(RIm)F complexes are *six-coordinate* and high-spin ($S = {}^5/_2$) for Por = the dianion of tetraphenylporphyrin (TPP) and protoporphyrin IX dimethyl ester (PPIXDME) and RIm = imidazole (HIm) and *N*-methylimidazole (MeIm).

Mechanistic investigations of reaction 1 showed that the kinetics depend markedly on the type of imidazole. Thus, changing from MeIm to HIm caused the rate to increase by a factor of ca. 100. Equally significant was the observation that the rate law also depends on the type of imidazole; e.g., the reaction of Fe(Por)Cl is second order in HIm but mixed first/zero order in MeIm. The mechanism outlined in eq 4–6 was proposed[10-14] to account for

$$Fe(Por)X + RIm \overset{K}{\rightleftharpoons} Fe(Por)(RIm)X \quad (4)$$

$$Fe(Por)(MeIm)X \xrightarrow{k} Fe(Por)(MeIm)^+X^- \xrightarrow[\text{fast}]{MeIm} Fe(Por)(MeIm)_2^+X^- \quad (5)$$

$$Fe(Por)(HIm)X + HIm \xrightarrow{k} Fe(Por)(HIm)_2^+X^- \quad (6)$$

the reactions of Fe(Por)Cl and Fe(Por)F. Very rapid (equilibrium) addition of RIm to Fe(Por)X generates Fe(Por)(RIm)X, which, with MeIm as the nucleophile, reacts via rate-determining X^- ionization. With HIm, however, a hydrogen-bonding interaction between the imidazole N–H and the departing X^- anion causes a rate acceleration and a change in the rate law; this interaction can be illustrated as

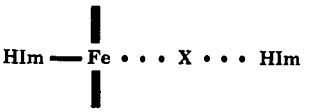

With $X^- = Cl^-$ the hydrogen bonding is a transition-state effect while it also occurs in the ground state when X^- is the more basic fluoride anion. Of course, such hydrogen bonding is not possible with MeIm. As expected, the rate (with MeIm or HIm) is accelerated by protic materials (H_2O, CF_3CH_2OH) and correlates to the hydrogen-bonding ability of the solvent as measured by Gutmann acceptor numbers.

The reactions described above are significant because of their relationship to interactions occurring in heme proteins. The relevant species from eq 1–3 is the transient Fe(Por)(RIm)X, which mimics the coordination in methemoglobin, metmyoglobin, and peroxidases with appropriate axial ligands. A relationship is also apparent with oxy-Hb and oxy-Mb when these are viewed as $Fe(III)-O_2^-$. The demonstrated importance of hydrogen bonding from an external imidazole in assisting the ionization of X^- in Fe(Por)(RIm)X clearly parallels distal-type hydrogen bonding believed to occur in heme proteins. For example, possible hydrogen bonding from the distal histidine to bound O_2 in HbO_2 and MbO_2 has been considered for many years[16] and recently

† University of Ulster.
‡ Brown University.

(1) Duclos, J. M. *Bioinorg. Chem.* **1973**, *2*, 263.
(2) Coyle, C. L.; Rafson, P. A.; Abbott, E. H. *Inorg. Chem.* **1973**, *12*, 2007.
(3) Ciaccio, P. R.; Ellis, J. V.; Munson, M. E.; Kedderis, G. L.; McConville, F. X.; Duclos, J. M. *J. Inorg. Nucl. Chem.* **1976**, *38*, 1885.
(4) Walker, F. A.; Lo, M.-W.; Ree, M. T. *J. Am. Chem. Soc.* **1976**, *98*, 5552.
(5) Adams, P. A.; Baldwin, D. A.; Hepner, C. E.; Pratt, J. M. *Bioinorg. Chem.* **1978**, *9*, 479.
(6) Yoshimura, T.; Ozaki, T. *Bull. Chem. Soc. Jpn.* **1979**, *52*, 2268.
(7) Momenteau, M. *Biochim. Biophys. Acta* **1973**, *304*, 814.
(8) Momenteau, M.; Rougee, M.; Loock, B. *Eur. J. Biochem.* **1976**, *71*, 63.
(9) Momenteau, M.; Mispelter, J.; Lexa, D. *Biochim. Biophys. Acta* **1973**, *320*, 652.
(10) Burdige, D.; Sweigart, D. A. *Inorg. Chim. Acta* **1978**, *28*, L131. Fiske, W.; Sweigart, D. A. *Inorg. Chim. Acta* **1979**, *36*, L429.
(11) Doeff, M. M.; Sweigart, D. A. *Inorg. Chem.* **1982**, *21*, 3699.
(12) Tondreau, G. A.; Sweigart, D. A. *Inorg. Chem.* **1984**, *23*, 1060.
(13) Jones, J. G.; Tondreau, G. A.; Edwards, J. O.; Sweigart, D. A. *Inorg. Chem.* **1985**, *24*, 296.
(14) Meng, Q.; Tondreau, G. A.; Edwards, J. O.; Sweigart, D. A. *J. Chem. Soc., Dalton Trans.* **1985**, 2269.
(15) Bond, A. M.; Sweigart, D. A. *Inorg. Chim. Acta* **1986**, *123*, 167.
(16) Pauling, L. *Nature (London)* **1964**, *203*, 182.

0020-1669/86/1325-4767$01.50/0

confirmed.[17,18] Presumably the hydrogen bonding is strong enough to provide stabilization but not so strong as to induce proton transfer and irreversible oxidation to HO_2 and Fe(III), although this may be occurring in the proton-dependent autooxidation and superoxide formation from MbO_2, HbO_2, and oxy-P450.[19] Oxygen binding to free iron and cobalt porphyrins is sensitive to hydrogen-bonding effects.[20-25] Orbital calculations based on X-ray data for iron and cobalt picket fence porphyrins show[26] a substantial attraction between the amide NH groups and bound O_2, even though the N(H)···O distance is rather long. By comparison of O_2, CO, and RNC binding to heme proteins and a chelated protoheme model, it was estimated that hydrogen bonding from the distal histidine to O_2 is favored by 1–2 kcal. Analogous hydrogen bonding probably occurs in met-Hb and met-Mb systems, and has been documented for met-MbCN.[27] Similarly, it is thought[28] that the distal histidine in cytochrome *c* peroxidase (CCP) hydrogen bonds to coordinated peroxide and so facilitates the heterolytic cleavage of the O–O bond to generate compound I; recent work with model hemes supports this suggestion.[29] Our work with Fe(Por)(RIm)X (X = Cl^-, F^-) and Co(Por)(RIm)X[30] (X = Cl^-, Br^-) models shows that hydrogen bonding lowers the free energy of activation for X^- dissociation by several kilocalories and that the effect follows the order of proton basicities: $F^- > Cl^- > Br^-$.

In eq 3 the spin changes from $S = {}^5/_2$ for Fe(Por)(RIm)X (X = Cl^-, F^-) to $S = {}^1/_2$ for Fe(Por)$(RIm)_2{}^+X^-$. The intermediate Fe(Por)$(RIm)^+X^-$, which is a good model for the transition state in eq 5 and 6, is known[31] to be high-spin. The Fe(Por)(RIm)X (X = Cl^-, F^-) models for distal-type hydrogen bonding differ from most protein systems in that the former are high spin. In order to study the role of spin state on axial ligand ionization and hydrogen-bonding effects and in order to study a system more closely related magnetically to the proteins, we selected reaction 7 for investigation. Previous thermodynamic work has shown[32]

$$Fe(TPP)N_3 + 2RIm \rightleftharpoons Fe(TPP)(RIm)_2{}^+N_3{}^- \qquad (7)$$

that MeIm reacts with $Fe(TPP)N_3$ to give the *low-spin* intermediate $Fe(TPP)(MeIm)N_3$, which converts to Fe(TPP)$(MeIm)_2{}^+N_3{}^-$ when a large excess of MeIm is present. The analogous HIm complex behaves similarly, except it is difficult to stop the reaction at the intermediate complex stage. The formation constant K_1 is much larger for $X = N_3{}^-$ than for X = Cl^- and F^- (vide infra); this is undoubtedly due to the low-spin nature of $Fe(TPP)(RIm)N_3$. We shall show that the mechanism of reaction 7 is the same as that for X = Cl^- and F^- and that hydrogen-bonding effects are important. However, the activation parameters for the rate-determining step in reactions 1 and 7 are very different, which is probably related to the different spin states of Fe(Por)(RIm)X. Also reported is the reduction electrochemistry of $Fe(TPP)(RIm)N_3$, obtained by low-temperature cyclic voltammetry.

Experimental Section

Special Precautions. A solution of $Fe(TPP)N_3$ in acetone is very susceptible to hydrolysis to $[Fe(TPP)]_2O$, and it is essential that all solvents be dry. A 10^{-6} M $Fe(TPP)N_3$ solution appears to hydrolyze in ca. 0.5 h, but solutions $\geq 10^{-5}$ M were stable for a day provided they were kept in the dark. Only porphyrin solutions showing no trace of the μ-oxo dimer (as judged by optical spectroscopy) were used for the physical studies. All glassware was oven-dried prior to use.

Materials. Linde 4A molecular sieves were dried in a vacuum oven at 200 °C for 4 h prior to use. AnalaR grade acetone was dried over sieves for 0.5 h, decanted over a fresh lot of sieves, and dried for another 0.5 h. The acetone was then filtered through a dried sintered-glass filter funnel and bottled and sealed immediately. Whether or not the acetone was then distilled had no effect on the results. Dichloromethane was distilled from calcium hydride. Imidazole was crystallized from ethanol and then sublimed in vacuum. *N*-Methylimidazole was dried over crushed KOH and then distilled from calcium hydride and kept over molecular sieves.

Synthesis of $Fe(TPP)N_3$. The procedure reported by Scheidt et al.[32] was followed with some modifications. $[Fe(TPP)]_2O$ (787 mg) was dissolved in benzene in a flask equipped with a magnetic stirrer and an addition funnel. NaN_3 (6.0 g) was dissolved in 100 mL of water and added to the flask. With vigorous stirring, 18 mL of concentrated H_2SO_4 was added dropwise. Stirring was continued for 1.5 h after which the organic phase was isolated and washed with water and dried with $MgSO_4$. The solution was then filtered and evaporated. The solid product was dried at room temperature in vacuum for 24 h. The spectrum of the product matched that previously reported[32] and showed no trace of the μ-oxo dimer. The yield was 92%. Anal. Calcd for $Fe(TPP)N_3$: C, 74.36; H, 3.97; N, 13.80. Found: C, 74.31; H, 4.02; N, 13.67.

Kinetic Studies. Stopped-flow experiments were performed with Dionex 110, Hi Tech SFL 210/S/961, and homemade instruments. The homemade stopped-flow device was made from Kel-F and Teflon and uses restraint of the driving syringes (rather than an independent stopping syringe). The apparatus has a common plunger driving two Teflon pistons (each with a central steel reinforcing spline) in a bored out Kel-F block. Also in the block is a double 3-way Teflon tap, spring loaded and able to sustain pressure. After the tap two 1-mm holes converge inside the block and come together against a eight-jet Milnes mixer, which is inset in a brass block drilled to accommodate it, and a quartz observation tube of 1.7-mm internal diameter. The Kel-F block, mixer, and quartz tube are held rigidly inside the brass block drilled to take thermostated water channels. The exit is a 0.5-mm-diameter hole drilled in a Teflon cylinder, which can be screwed against the quartz tube, making all internal connections tight. The observation channel drilled in the brass block is 2 mm in diameter and at righ angles to the reactant flow, 0.5 cm after the mixer. Light from a 50-W projector lamp with a stabilized power supply is focused through a 0.2-mm slit and a diffraction grating, through the reaction chamber, and onto a photomultiplier tube. In our experiments the output signal was fed to a Bryans Transcribe 2000 recorder for processing. The dead time of the instrument is 2 ms, and results are comparable to those obtained from commercial instruments.

Kinetic runs with MeIm were inconveniently slow for the stopped-kflow method and a Perkin-Elmer 124 instrument was used. In order to measure the small optical density changes at low MeIm concentrations (vide infra), fairly high concentrations of $Fe(TPP)N_3$ were used (ca. 8 $\times 10^{-5}$ M) and a difference method employed. The reference cell was filled with a $\simeq 8 \times 10^{-5}$ M $Fe(TPP)N_3$ solution diluted 50/50 with dry acetone. The sample cell contained 1.5 mL of undiluted $Fe(TPP)N_3$ solution and 1.5 mL of MeIm, which was injected with a syringe fitted with a cannula. The absorbance was then followed at the appropriate wavelength (usually 445 nm). In all experiments the temperature was controlled to ±0.1 °C.

Equilibrium Studies. These were performed in such a way that a stock solution of porphyrin ($\simeq 5 \times 10^{-5}$) was diluted 50/50 with RIm solution and the maximum and final optical densities for a series of such mixtures were monitored on the stopped-flow (HIm) or a conventional double-beam instrument (MeIm). The reactant spectrum was taken at the

(17) Phillips, S. E. V.; Schoenborn, B. P. *Nature (London)* **1981**, *292*, 81.
(18) Shaanan, B. *Nature (London)* **1982**, *296*, 683.
(19) Wallace, W. J.; Maxwell, J.; Caughey, W. S. *Biochem. Biophys. Res. Commun.* **1974**, *57*, 1104. Misra, H. P.; Fridovich, I. *J. Biol. Chem.* **1972**, *247*, 6960. Gotoh, T.; Shikama, K. *J. Biochem. (Tokyo)* **1976**, *80*, 397. Demma, L. S.; Salhany, J. M. *J. Biol. Chem.* **1979**, *252*, 1226. Demma, L. S.; Salhany, J. M. *J. Biol. Chem.* **1979**, *254*, 4532. Mansouri, A.; Winterhalter, K. H. *Biochemistry* **1973**, *12*, 4946. Dolphin, D.; James, B. R.; Welborn, H. C. *J. Mol. Catal.* **1980**, *7*, 201.
(20) Jameson, G. B.; Ibers, J. A. *Comments Inorg. Chem.* **1983**, *2*, 97.
(21) Collman, J. P.; Brauman, J. I.; Iverson, B. L.; Sessler, J. L.; Morris, R. M.; Gibson, Q. H. *J. Am. Chem. Soc.* **1983**, *105*, 3052.
(22) Suslick, K. S.; Fox, M. M. *J. Am. Chem. Soc.* **1983**, *105*, 3507.
(23) Suslick, K. S.; Fox, M. M.; Reinert, T. J. *J. Am. Chem. Soc.* **1984**, *106*, 4522.
(24) Momenteau, M.; Lavalette, D. *J. Chem. Soc., Chem. Commun.* **1982**, 341. Mispelter, J.; Momenteau, M.; Lavalette, D.; Lhoste, J.-M. *J. Am. Chem. Soc.* **1983**, *105*, 5165. Lexa, D.; Momenteau, M.; Rentien, P.; Rytz, G.; Saveant, J.-M.; Xu, F. *J. Am. Chem. Soc.* **1984**, *106*, 4755. Lavalette, D.; Tetreau, C.; Mispelter, J.; Momenteau, M.; Lhoste, J.-M. *Eur. J. Biochem.* **1984**, *145*, 555.
(25) Dokuzovic, Z.; Ahmeti, X.; Pavlovic, D.; Murati, I.; Asperger, S. *Inorg. Chem.* **1982**, *21*, 1576.
(26) Jameson, G. B.; Drago, R. S. *J. Am. Chem. Soc.* **1985**, *107*, 3017.
(27) Morishima, I.; Hara, M. *J. Am. Chem. Soc.* **1982**, *104*, 6833.
(28) Poulos, T. L.; Kraut, J. *J. Biol. Chem.* **1980**, *255*, 8199. Poulos, T. L.; Freer, S. T.; Alden, R. A.; Edwards, S. L.; Skogland, U.; Takio, K.; Eriksson, B.; Xuong, N.; Yonetani, T.; Kraut, J. *J. Biol. Chem.* **1980**, *255*, 575.
(29) Traylor, T. G.; Lee, W. A.; Stynes, D. V. *J. Am. Chem. Soc.* **1984**, *106*, 755.
(30) Mahmood, A.; Jones, J. G.; Edwards, J. O.; Sweigart, D. A., unpublished results.
(31) Quinn, R.; Nappa, M.; Valentine, J. S. *J. Am. Chem. Soc.* **1982**, *104*, 2588.
(32) Adams, K. M.; Rasmussen, P. G.; Scheidt, W. R.; Hatano, K. *Inorg. Chem.* **1979**, *18*, 1892.

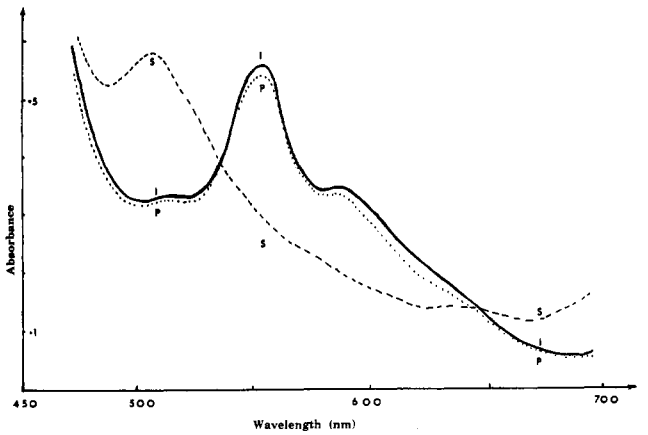

Figure 1. Reaction of 2×10^{-5} M $Fe(TPP)N_3$ with 5×10^{-3} M HIm in acetone at −78 °C: (S, - -) solution of $Fe(TPP)N_3$ before reaction; (I, —) solution of $Fe(TPP)N_3$ with HIm present at −78 °C; (P, ···) solution used for I after it was warmed to room temperature for several minutes and recooled to −78 °C.

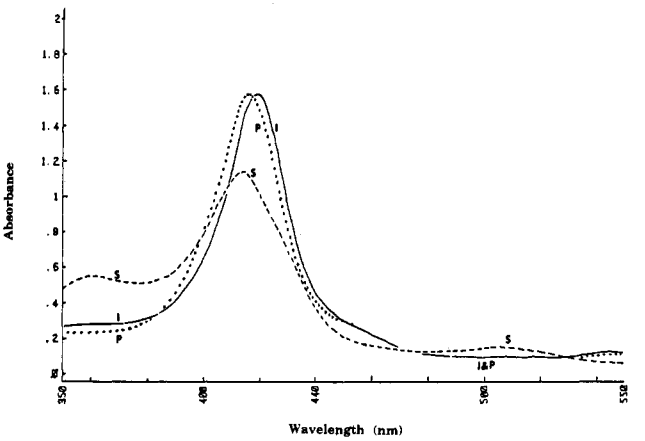

Figure 2. Reaction of 10^{-5} M solution of $Fe(TPP)N_3$ with 0.01 M HIm in acetone at 25 °C. (S, - -) solution of $Fe(TPP)N_3$ before reaction; (I, —) solution of $Fe(TPP)N_3$ within first 0.1 s after adding the HIm; (P, ···) solution used for I 5 min after mixing.

beginning and end of each series of measurements. The range of HIm concentrations used to determine K_1 was 5×10^{-5} to 5×10^{-3} M, and for K_2 determinations from 1×10^{-2} to 2×10^{-1} M. With MeIm the range of concentrations used for K_2 measurements was 0.05–1.0 M. Solution preparations with MeIm were performed in a drybox.

Other Studies. Low-temperature optical spectra and variable-temperature conductivity measurements were made as previously described.[12] Low-temperature cyclic voltammetry was done with EG&G 362 and BAS CV 27 potentiostats. The supporting electrolyte was tetrabutylammonium perchlorate (TBAP). The reference electrode was Ag/AgCl in CH_2Cl_2 with 0.1 M TBAP and was saturated with LiCl. A platinum wire and disk functioned as the counter and working electrodes, respectively. Further procedural details concerning the low-temperature electrochemical measurements have recently been published.[15]

Results and Discussion

Characterization of Fe(TPP)(RIm)N_3. Scheidt et al.[32] reported base addition to $Fe(TPP)N_3$ in dichloromethane. With pyridine as the base they isolated $Fe(TPP)(py)N_3$ and characterized it via X-ray diffraction and magnetic susceptibility studies, which showed that this complex is six-coordinate and low spin. Spectroscopic studies with HIm and MeIm suggested that analogous low-spin species form. Equilibrium constants K_1 were evaluated, although the value for the HIm complex was only approximate because $Fe(TPP)(HIm)N_3$ could not be generated in the absence of $Fe(TPP)(HIm)_2^+N_3^-$.

We found that $Fe(TPP)N_3$ in dry acetone has a optical spectrum similar to that of the well-studied Fe(TPP)Cl. In the presence of excess RIm the spectrum is very much like that of $Fe(TPP)(RIm)_2^+Cl^-$. Spectra recorded at −78 °C in a previously described[12] special cell allowing mixing of solutions at low temperatures showed clearly that the addition of HIm and MeIm to $Fe(TPP)N_3$ occurs rapidly to give a species that is stable indefinitely at low temperatures but converts to $Fe(TPP)(RIm)_2^+N_3^-$ upon warming and recooling. In the 500–750-nm region the intermediate has a spectrum very similar to that for low-spin $Fe(TPP)(RIm)_2^+N_3^-$, however, there are small spectral differences that are reproducible and definitely real. Figure 1 illustrates some results. The conclusion is that $Fe(TPP)N_3$ reacts rapidly with RIm even at −78 °C to give a low-spin intermediate that converts only slowly to $Fe(TPP)(RIm)_2^+N_3^-$. The first step involves large spectral changes, the second step only small ones. Quantitative treatment of the spectral data (vide infra) show that the intermediate is $Fe(TPP)(RIm)N_3$, as expected. These findings were duplicated at 25 °C by using a Hewlett Packard diode array spectrometer, which can obtain the entire spectrum within 0.1 s. A large change in the spectrum occurred upon mixing the reactants; this was followed by a slow spectral change. These investigations were extended to the 350–550-nm region where addition of, e.g., 0.05 M HIm immediately produced the large spectral changes shown in Figure 2. The initial changes were followed by a further small decrease in absorbance in the 360-nm region and a small shift in the position of the Soret maximum. With 0.01 M HIm, $Fe(TPP)(HIm)N_3$ is fully formed but the transition to final product is not complete at equilibrium. This indicates that $K_1 > K_2$, opposite to that found with Fe(TPP)X ($X = Cl^-, F^-$).

Table I. Electrochemical Data for Fe(III)/Fe(II) Reductions in Dichloromethane[a]

complex	T/°C	$E_{1/2}$/V[b]
$Fe(TPP)N_3$	20	−0.47 (100)
$Fe(TPP)N_3$	−91	−0.44 (110)
$Fe(TPP)(MeIm)_2^+N_3^-$	20	−0.20 (80)
$Fe(TPP)(MeIm)_2^+N_3^-$	−90	−0.19 (70)
$Fe(TPP)(HIm)_2^+N_3^-$	15	−0.29 (80)
$Fe(TPP)(HIm)_2^+N_3^-$	−90	−0.27 (70)
$Fe(TPP)(MeIm)N_3$	−90	−0.59[c]
$Fe(TPP)(HIm)N_3$	−90	−0.59[c]
$Fe(TPP)(HIm)N_3$[d]	−93	−0.65[c]
Fe(TPP)(MeIm)Cl	−85	−0.55[c,e]

[a] Scan rate = 100 mV/s; 0.05 M TBAP present; concentrations were [porphyrin] $\simeq 1 \times 10^{-3}$ M, [HIm] = 0.05 M, and [MeIm] = 0.2 M. [b] $E_{1/2}$ taken as $(E_p^{red} + E_p^{ox})/2$. Numbers in parentheses are peak separations in millivolts. $E_{1/2}$ for ferrocene at 20 °C was +0.46 V. [c] Chemically irreversible—the value listed is the peak potential E_p^{red}. [d] Contains [phen] = 0.1 M. [e] From ref 15.

Conductivity experiments in acetone and dichloromethane at −78 °C showed that $Fe(TPP)(RIm)N_3$ like $Fe(TPP)N_3$ is essentially nonconducting. Thus, HIm or MeIm added to a solution of $Fe(TPP)N_3$ caused very little change in conductivity. Warming to room temperature and recooling caused the conductivity to increase markedly, as expected for the ionic product $Fe(TPP)(RIm)_2^+N_3^-$. Analogous results were previously found[12] with Fe(TPP)(RIm)Cl and this clearly points to $Fe(TPP)(RIm)N_3$ as being six-coordinate, as already inferred from spectral similarities between $Fe(TPP)(RIm)_2^+N_3^-$ and $Fe(TPP)(py)N_3$. The latter complex is known[32] to be six-coordinate from a crystal structure.

Low-temperature cyclic voltammetry was also used to characterize $Fe(TPP)(RIm)N_3$. Table I and Figure 3 give relevant data. The CV's were obtained by cooling a dichloromethane solution of $Fe(TPP)N_3$ to ca. −90 °C and then adding ca. 0.05 mL of a concentrated solution of RIm via a gastight syringe. The first scan in Figure 3 shows a chemically irreversible wave (wave 1) that is due to the reduction of $Fe(TPP)(HIm)N_3$. Once reduced, azide is rapidly lost and $Fe(TPP)(HIm)_2$ is formed, accounting for oxidation wave 2. Wave 3 represents reduction of $Fe(TPP)(HIm)_2^+$, which reaches a steady-state concentration at the electrode after several scans. As expected, warming the solution to room temperature and recooling causes wave 1 to vanish and only the waves for the 2/3 couple to remain. Entirely analogous results were obtained with MeIm. This behavior closely parallels the chemistry of the Fe(TPP)Cl/RIm system[15] except

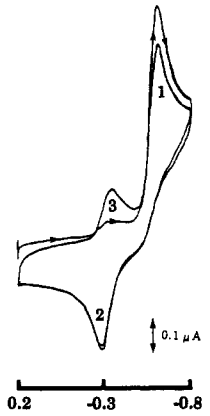

Figure 3. Cyclic voltammogram of ca. 10^{-4} M Fe(TPP)(HIm)N_3 in dichloromethane at −91 °C. The scan rate was 100 mV/s.

that the Fe(TPP)(RIm)X intermediates are considerably more stable for X = N_3^-. The (relative) thermal stability of Fe(TPP)(HIm)N_3 at low temperature allowed us to probe the effect of hydrogen bonding from the coordinated HIm to a base. Thus, the addition of 0.1 M phen caused the E_p value to shift from −0.59 to −0.65 V. This negative shift is small but significant and is most likely due to hydrogen bonding from the imidazole N–H to phen being stronger in the Fe(III) oxidation state as compared to the Fe(II) state. Such proximal hydrogen bonding has the effect of increasing the electron density on the iron and thereby making it more difficult to reduce. Analogous hydrogen-bonding effects have been previously explored by us[33] with Fe(Por)$(HIm)_2^+$ complexes; the present example is probably more significant since most Fe(III) heme proteins have only one proximal histidine. The conclusion is that variation of proximal histidine hydrogen bonding is an entirely feasible way for heme proteins to modulate redox potentials.

The electrochemistry of Fe(TPP)N_3 at low temperature proved to be quite interesting. Previous work with Fe(TPP)X complexes at room temperature established[34] eq 8 and 9 as the major pro-

$$\mathrm{Fe(TPP)X} + e^- \rightleftharpoons \mathrm{Fe(TPP)} + \mathrm{X}^- \quad (8)$$

$$\mathrm{Fe(TPP)} + e^- \rightleftharpoons \mathrm{Fe(TPP)}^- \quad (9)$$

cesses with X = Cl^- and N_3^-. Figure 4 shows the CV's of Fe(TPP)N_3 as a function of temperature. Waves 1/2 correspond to the couple in eq 8. At room temperature N_3^- rapidly dissociates as Fe(TPP)N_3 is reduced and the product Fe(TPP) gives rise to the waves 3/4 (eq 9). However, Figure 4 shows that the 3/4 couple almost vanishes at −91 °C while the 1/2 couple remains. The obvious interpretation is that azide dissociation from Fe(TPP)N_3^- is slow at low temperature so that Fe(TPP) is not formed within the time scale of cyclic voltammetry. This behavior contrasts with that of Fe(TPP)Cl^-, which dissociates chloride fairly rapidly even at low temperature.[15] These observations are consistent with kinetic studies (vide infra) showing that azide dissociates much more slowly than does chloride from Fe(TPP)(RIm)X. Our electrochemical results nicely illustrate the utility of low-temperature cyclic voltammetry, especially in relatively nonpolar solvents like dichloromethane.

Equilibrium Studies. By measuring equilibrium optical densities, it is in principle possible to determine the stepwise formation constants K_1 and K_2 (eq 2 and 3) for Fe(TPP)$(RIm)_2^+N_3^-$. In practice it is difficult to calculate reliable values for K_1 and K_2 by this procedure due to the small optical density change for the second step and the fact that both equilibria must be considered simultaneously. Scheidt et al.[32] encountered similar difficulties in trying to determine K_1 and K_2 for reaction 7 in dichloromethane;

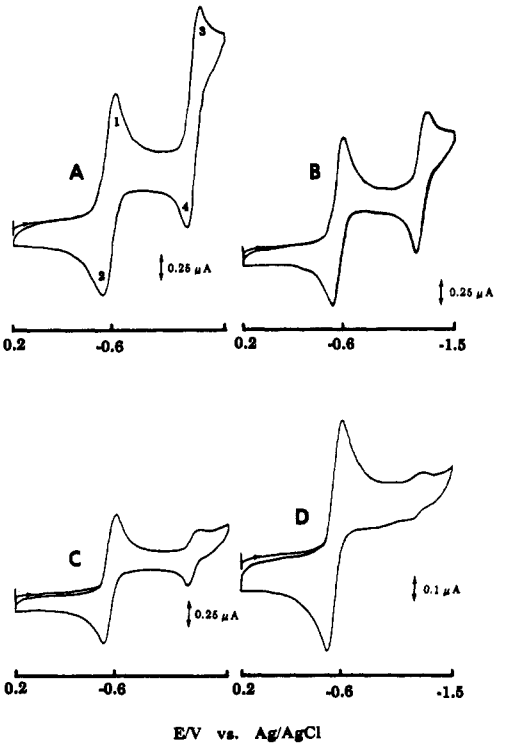

Figure 4. Cyclic voltammograms of ca. 10^{-4} M Fe(TPP)N_3 in dichloromethane at (A) 20, (B) −45, (C) −70, and (D) −90 °C. The scan rate was 100 mV/s.

Table II. Equilibrium Constants for Reactions 2 and 3 in Acetone at 25 °C

complex	RIm	K_1/M^{-1}	K_2/M^{-1}	$10^{-3}\beta^2/M^{-2}$
Fe(TPP)N_3	MeIm	800 ± 100	6 ± 1	4.8
Fe(TPP)N_3	HIm	1300 ± 300	37 ± 7	48
Fe(TPP)Cl[a]	MeIm	3.9 ± 0.3	1700 ± 400	6.6
Fe(TPP)Cl[a]	HIm	13 ± 2	12000 ± 3000	160
Fe(TPP)F[b]	HIm	20 ± 5	800 ± 250	17

[a] From ref 11 and 12. [b] From ref 13.

the only good constants they were able to extract were K_1 for MeIm and the product $K_1K_2 = \beta_2$ for HIm.

However, our finding that the K_1 step (eq 2) is very rapid and that the K_2 step is relatively slow for both HIm and MeIm means that it is possible to measure the equilibrium constants for each step *separately* if a wavelength is chosen where substantial optical density changes are seen for both steps. This proved to be the case in the 440–445-nm region of the spectrum, where the first step leads to an increased absorbance and the second to a decreased absorbance. For the first step K_1 was calculated from a Wardley–Hammick–Foster plot, eq 10, in which $\Delta A = A - A_0$, where

$$\Delta A/[\mathrm{RIm}] = -K\Delta A + Ka\Delta\epsilon \quad (10)$$

A is the absorbance of the equilibrium mixture and A_0 is that of Fe(TPP)N_3 in the absence of RIm. The quantity a is the total porphyrin concentration and $\Delta\epsilon$ is the extinction coefficient difference between the product and reactant. Note that $\Delta\epsilon$ need not be known to utilize eq 10. Figure 5 shows the plot for HIm. Experimentally, the absorbance A was readily determined by extrapolating the stopped-flow output back to zero time, which eliminates any contribution due to the second step (the first step is instantaneous on the stopped-flow time scale). This procedure is quite accurate because the K_2 step is relatively slow (vide infra). Equation 10 was also used to calculate K_2; in this case A_0 refers to the absorbance of Fe(TPP)(RIm)N_3 and A to the absorbance of equilibrium mixture defined by eq 3. Because $K_1 >> K_2$, [RIm] could be adjusted so that Fe(TPP)(RIm)N_3 was completely formed while the second RIm addition was far from complete. Hence A_0 could be accurately determined. Figure 6 shows a plot for MeIm, and Table II summarizes the results. Comparing

(33) Doeff, M. M.; Sweigart, D. A.; O'Brien, P. *Inorg. Chem.* **1983**, *22*, 851. O'Brien, P.; Sweigart, D. A. *Inorg. Chem.* **1985**, *24*, 1405.
(34) Bottomley, L. A.; Kadish, K. M. *Inorg. Chem.* **1981**, *20*, 1348.

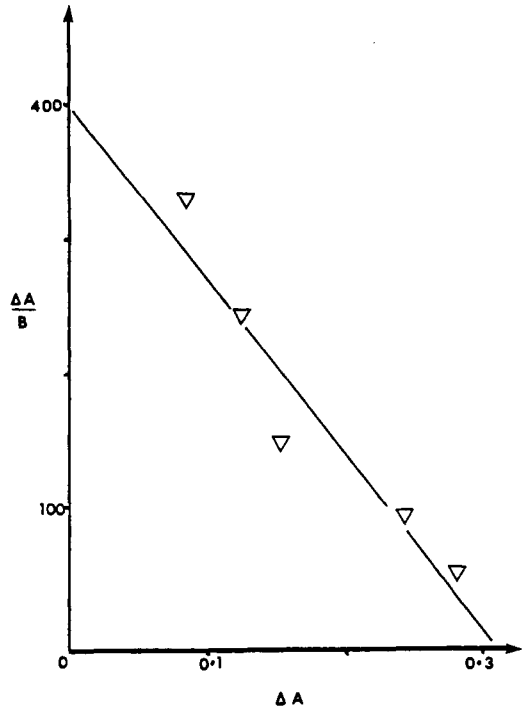

Figure 5. Plot of eq 10 for the determination of K_1 for the reaction $Fe(TPP)N_3 + HIm \rightarrow Fe(TPP)(HIm)N_3$ in acetone at 25 °C. The base B is HIm.

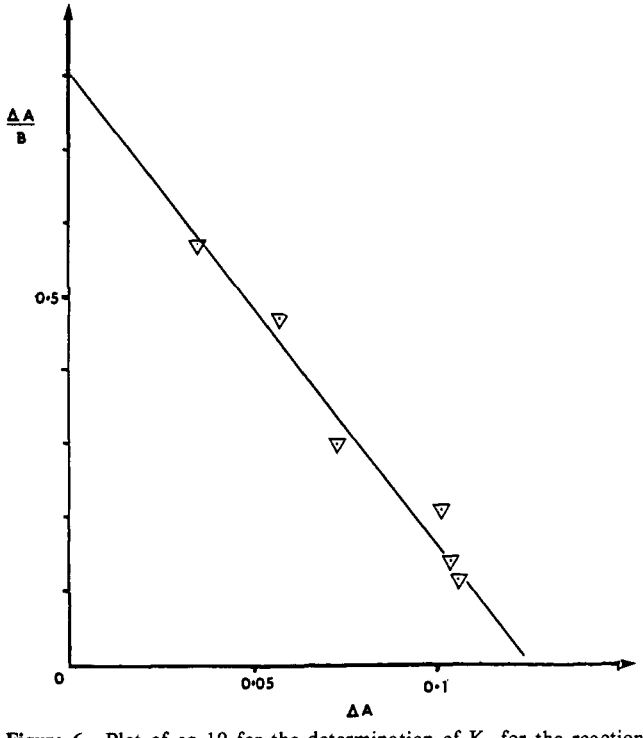

Figure 6. Plot of eq 10 for the determination of K_2 for the reaction $Fe(TPP)(MeIm)N_3 + MeIm \rightarrow Fe(TPP)(MeIm)_2^+N_3^-$ in acetone at 25 °C. The base B is MeIm.

Fe(TPP)Cl and $Fe(TPP)N_3$, Table II, shows that the overall stability constant (β_2) is roughly the same for a given RIm. However, because of the different spin states of the intermediate complexes, $K_1 << K_2$ for the former while $K_1 >> K_2$ for the latter.

Kinetic Studies. The addition of RIm to $Fe(TPP)N_3$ to give $Fe(TPP)(RIm)N_3$ was too rapid to follow by the stopped-flow technique at 25 °C. The second step (eq 3) with HIm was conveniently followed via the stopped-flow method. With MeIm a standard spectrophotometer was used. Under some reaction conditions both techniques were used, and the rate constants

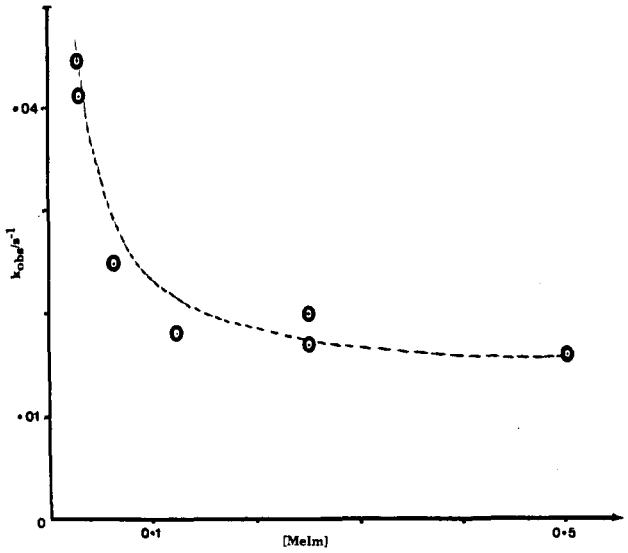

Figure 7. Rate profile for the reaction of MeIm with $Fe(TPP)N_3$ in acetone at 25 °C.

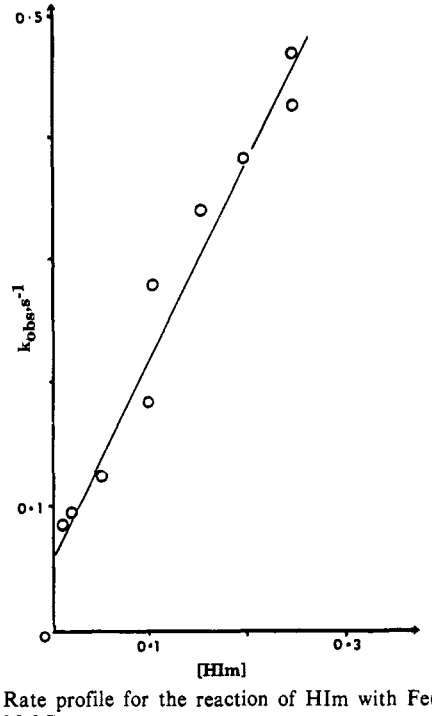

Figure 8. Rate profile for the reaction of HIm with $Fe(TPP)N_3$ in acetone at 25 °C.

obtained agreed closely. Experiments were always done with a large excess of RIm over the porphyrin concentration, which was in the range $(0.5–5.0) \times 10^{-5}$ M. Pseudo-first-order rate constants, k_{obsd}, were calculated in the usual way. Plots of k_{obsd} vs. RIm concentration are given in Figure 7 and 8, which show that MeIm and HIm give distinctly different rate behavior. With MeIm, k_{obsd} is seen to be independent of [MeIm] except at low nucleophile concentrations when k_{obsd} increases. While an increase in k_{obsd} as [MeIm] is lowered might seem peculiar; in fact this is readily understood within the context of the proposed mechanism, eq 11–13. This mechanism yields eq 14 for k_{obsd}, which can be

$$Fe(TPP)N_3 + MeIm \overset{K_1}{\rightleftharpoons} Fe(TPP)(MeIm)N_3 \quad (11)$$

$$Fe(TPP)(MeIm)N_3 \underset{k_2}{\overset{k_1}{\rightleftharpoons}} Fe(TPP)(MeIm)^+N_3^- \quad (12)$$

$$Fe(TPP)(MeIm)^+N_3^- + MeIm \underset{k_4}{\overset{k_3}{\rightleftharpoons}} Fe(TPP)(MeIm)_2^+N_3^- \quad (13)$$

$$k_{obsd} = \left(\frac{k_1K_1[MeIm]}{1 + K_1[MeIm]}\right)\left(\frac{k_3[MeIm]}{k_2 + k_3[MeIm]}\right) + \frac{k_2k_4}{k_2 + k_3[MeIm]} \quad (14)$$

accurately approximated by eq 15 since it is known that $K_1 = 800$

$$k_{obsd} = \frac{k_1k_3[MeIm]}{k_2 + k_3[MeIm]} + \frac{k_2k_4}{k_2 + k_3[MeIm]} \quad (15)$$

M^{-1} (Table II), so that $K_1[MeIm] >> 1$ under the conditions used. Equation 15 predicts limits of k_4 and k_1 as [MeIm] gets very small and large, respectively. The reason k_{obsd} rises at low [MeIm] is simply because $k_4 > k_1$. In other words, k_{obsd} measures the rate of approach to equilibrium, and in this case, the reverse contributes significantly. Since $K_2 = k_1k_3/k_2k_4 = 6\ M^{-1}$ (Table II) and $k_4 > k_1$, we can conclude that $k_3 >> k_2$. With the assumption $k_3[MeIm] >> k_2$, k_{obsd} can be further approximated as eq 16. A

$$k_{obsd} = k_1 + \frac{k_2k_4}{k_3[MeIm]} \quad (16)$$

plot of k_{obsd} vs. $1/[MeIm]$ should give K_2 as the intercept divided by the slope. Such a plot is reasonably linear (correlation coefficient = 0.99) and yields $K_2 = 10 \pm 5\ M^{-1}$. This value agrees well with the K_2 measured under equilibrium conditions ($K_2 = 6$; Table II), especially in view of the fact that the k_{obsd} values at low [MeIm] are of only moderate precision because of small optical density changes. The most important conclusions for this reaction are that (1) k_1, the rate constant for azide ionization, equals $0.017\ s^{-1}$ at 25 °C and (2) the rate law in the forward direction is found to rapidly approach zero order in MeIm. The temperature dependence of k_1 was calculated from k_{obsd} measurements at [MeIm] = 0.5 M at four temperatures between 15 and 45 °C. The standard Eyring plot was highly linear and yielded $\Delta H^\ddagger = 16.6 \pm 0.7$ kcal mol^{-1} and $\Delta S^\ddagger = -10 \pm 2$ cal deg^{-1} mol^{-1}.

The results of a study of reaction 7 with HIm as the nucleophile are shown in Figure 8. The observed behavior at 25 °C obeys the equation $k_{obsd}/s^{-1} = 1.5[HIm] + 0.06$. Within the context of the above discussion the simplest mechanism is given by eq 17 and 18, which predict eq 19 for k_{obsd}. From the known value of

$$Fe(TPP)N_3 + HIm \underset{}{\overset{K_1}{\rightleftharpoons}} Fe(TPP)(HIm)N_3 \quad (17)$$

$$Fe(TPP)(HIm)N_3 + HIm \underset{k_2}{\overset{k_1}{\rightleftharpoons}} Fe(TPP)(HIm)_2{}^+N_3{}^- \quad (18)$$

$$k_{obsd} = \frac{k_1K_1[HIm]^2}{(1 + K_1[HIm])} + k_2 \quad (19)$$

K_1 (Table II) the approximation $K_1[HIm] >> 1$ is good, which leads to eq 20. Accordingly, the slope/intercept in Figure 8 is

$$k_{obsd} = k_1[HIm] + k_2 \quad (20)$$

interpreted as $k_1/k_2 = K_2$. This ratio is $1.5/0.06 = 25 \pm 20\ M^{-1}$, which is in acceptable agreement with K_2 determined under equilibrium conditions ($K_2 = 37 \pm 7$; Table II). As was thoroughly documented[11-14] with Fe(TPP)X (X = Cl^-, F^-), we propose that the primary mechanistic difference between MeIm and HIm in reaction 7 is hydrogen bonding by HIm to the developing azide ion in eq 18. This simple interaction accounts for the differing rate laws (eq 15 and 20) and the qualitative observation that the reaction is much faster with HIm compared to MeIm. Equation 18 assumes that the hydrogen bonding occurs in the transition state and not in the ground state for the k_1 step. There was no spectroscopic or kinetic evidence of hydrogen bonding in the ground state for the reactions of Fe(TPP)Cl and Fe(TPP)N_3. With Fe(TPP)F, however, there was evidence of ground-state hydrogen bonding by external HIm to Fe(TPP)(HIm)F.[13] The important point, however, is that hydrogen bonding to the departing X^- anion in Fe(TPP)(HIm)X is a prominent feature for all three anions. The combined influence of the preequilibrium (K_1) and hydrogen bonding in the transition state (and in one case the ground state) of Fe(TPP)(HIm)X is to make the experimentally observed limiting rate laws first order in HIm for N_3^-, second order for Cl^-, and zero order for F^-. In spite of this kinetic diversity there exists mechanistic unity for the three reactions.

The complete kinetic profile of the reaction of Fe(TPP)N_3 with HIm was determined at six temperatures between 15 and 45 °C. An Eyring plot for k_1 gave $\Delta H^\ddagger = 19.4 \pm 0.8$ kcal mol^{-1} and $\Delta S^\ddagger = +9 \pm 2.5$ cal deg^{-1} mol^{-1}. Similar treatment of the k_2 constants was subject to errors too large to yield meaningful activation parameters.

The effect of external hydrogen bonders on the rate of reaction 7 with MeIm was investigated by using trifluoroethanol (TFE). With [MeIm] fixed at 0.1 or 0.5 M and [TFE] in the range 0.01–0.10 M, the azide ionization rate (eq 12) at 25 °C followed the relation $k_{obsd}/s^{-1} = 1.0[TFE] + 0.02$. The slope of 1.0 M^{-1} s^{-1} can be compared to the slope of 1.5 M^{-1} s^{-1} for HIm in eq 20, the conclusion being that HIm and TFE are very similar with respect to acceleration of azide ionization via hydrogen bonding. With the analogous Fe(TPP)Cl reactions the slopes are 300 M^{-1} s^{-1} and 450 M^{-1} s^{-1}, respectively. These are in the same ratio found for Fe(TPP)N_3. Quantitative consideration of the effect of TFE is somewhat complicated by hydrogen-bonding interactions with the MeIm nucleophile; variation of the –OH chemical shift in TFE as a function of MeIm concentration suggested that the association constant for this hydrogen bonding is $1.2 \pm 0.1\ M^{-1}$.

Comparative Behavior of M(Por)X Complexes. Table III provides a summary of all available and relevant data for reaction 1. Regardless of the metal (Fe, Co), anion (F^-, Cl^-, Br^-, N_3^-), or porphyrin ring (TPP, PPIXDME, PPIX) the general mechanism outlined by eq 4–6 fits the data accurately. The general reactivity sequence for anion ionization from M(Por)(RIm)X (rate constant k) is: Fe(PPIX)Cl > Fe(PPIXDME)Cl ≃ Fe(TPP)Cl ≃ Fe(TPP)F > Co(TPP)Br ≃ Fe(TPP)N_3 > Co(TPP)Cl. Although the reactions with MeIm and HIm feature very different rates and rate laws, strong support for the assertion that the rate-limiting step is anion ionization for both series of reactions is provided by a LFER between log k_{HIm} and log k_{MeIm} for the five metalloporphyrins studied with both nucleophiles. This LFER (correlation coefficient = 0.98) has the form $\log k_{HIm} = \log k_{MeIm} + 2.1$.

In order to make a comparison of the results for M(Por)Cl and Fe(TPP)N_3, it is necessary to know what spin changes occur during the reactions with RIm. The sequence of pertinent species is M(Por)X → M(Por)(RIm)X → M(Por)(RIm)$^+X^-$ → M(Por)(RIm)$_2{}^+X^-$. With M = Fe and X = Cl^- it has been established[10-14,31,35] that the spin changes are $S = {}^5/_2 \rightarrow {}^5/_2 \rightarrow {}^5/_2 \rightarrow {}^1/_2$. Especially relevant is the spin state of M(Por)(RIm)$^+X^-$, which should be similar structurally to the activated complex for the rate-determining X^- ionization step discussed above. Thus for Fe(Por)Cl complexes there is no spin change during the rate-limiting step. With Co(Por)Cl the spin is $S = {}^1/_2$ for all species in the reaction sequence,[36] so again there is no spin change during the rate limiting step. Fe(TPP)N_3 is different in that the spin changes are $S = {}^5/_2 \rightarrow {}^1/_2 \rightarrow {}^5/_2 \rightarrow {}^1/_2$; i.e., there are *three* spin changes during the reaction.[31,32,35] One manifestation of this can be seen in the relatively large K_1 values for Fe(TPP)(RIm)N_3 compared to Fe(Por)(RIm)Cl. The $S = {}^5/_2 \rightarrow {}^1/_2$ spin change involved in the formation of the former complex means that there should be a substantial favorable contribution from crystal field stabilization energy (CFSE) effects.

Only for Fe(TPP)N_3 is there a spin change during the rate-determining step. It is therefore important to explore how this would be expected to influence the rate and activation parameters. Table III shows that $\Delta S_k^\ddagger$ is remarkably constant (−22 ± 2 eu)

(35) Scheidt, W. R.; Geiger, D. K.; Lee, Y. J.; Reed, C. A.; Lang, G. *J. Am. Chem. Soc.* **1985**, *107*, 5693.
(36) Sakurai, T.; Yamamoto, K.; Naito, H.; Nakamoto, N. *Bull. Chem. Soc. Jpn.* **1976**, *49*, 3042. Yamamoto, K.; Uzawa, J.; Chijimatsu, T. *Chem. Lett.* **1979**, 89. Lauher, J. W.; Ibers, J. A. *J. Am. Chem. Soc.* **1974**, *96*, 4447. Gouedard, M.; Gaudemer, F.; Gaudemer, A.; Riche, C. *J. Chem. Res., Synop.* **1978**, 30.

Table III. Comparison of Rate and Thermodynamic Data for the Reaction of M(Por)X with RIm[a]

M(Por)	X^-	RIm	K^b	k^c	kK	$\Delta H_k^\ddagger$	$\Delta S_k^\ddagger$
Fe(TPP)	N_3^-	MeIm	800	0.017	14	16.6	−10
Fe(TPP)	N_3^-	HIm	1300	1.5	1950	19.4	+9
Fe(TPP)	Cl^-	MeIm	3.9	3.5	14	9.7	−24
Fe(TPP)	Cl^-	HIm	13	450	5900	≈11	≈−10
Fe(PPIXDME)	Cl^-	MeIm	1.8	2.8	5.0	10.5	−20
Fe(PPIXDME)	Cl^-	HIm	9.0	580	5200		
Fe(PPIX)	Cl^-	MeIm	13	30	390	9.3	−21
Fe(PPIX)	Cl^-	HIm			110000		
Fe(TPP)	F^-	HIm	20	450	9000		
Co(TPP)[d]	Cl^-	MeIm		0.00060		15.4	−20
Co(TPP)[d]	Cl^-	HIm		0.25			
Co(TPP)[d]	Br^-	MeIm		0.025			
Co(TPP)[d]	Br^-	HIm		1.6			

[a] All data refer to 25 °C in acetone; data for Fe–Cl and Fe–F complexes from ref 10–14. Units for $\Delta H^\ddagger$ are kcal mol^{-1} and for $\Delta S^\ddagger$ are cal deg^{-1} mol^{-1}. [b] Defined by eq 4; also termed K_1 in text; units are M^{-1}. [c] Refers to ionization rate constant as in eq 5 and 6; also termed k_1 in text; units are s^{-1} for MeIm and M^{-1} s^{-1} for HIm. [d] From ref 30.

for MeIm reacting with Fe(TPP)Cl, Fe(PPIX)Cl, Fe(PPIXDME)Cl, and Co(TPP)Cl; none of these reactions involves a spin change during the ionization step. With Fe(TPP)N_3, however, $\Delta S_k^\ddagger$ for the MeIm reaction is −10 eu. Similarly, the reaction with HIm has a much more positive $\Delta S_k^\ddagger$ value for Fe(TPP)N_3 (+9 eu) compared to that for Fe(TPP)Cl (≈−10 eu). That $\Delta S_k^\ddagger$ is relatively more positive with HIm compared to MeIm is probably not linked to the spin change since it also occurs with Fe(TPP)Cl and has been explained[14] previously as due to hydrogen bonding by HIm to the departing anion, which releases solvent molecules hydrogen bonded to the HIm and reduces the number of solvent molecules required to solvate the X^- anion.

Various estimates are available for the thermodynamics of a $S = {}^1/_2 \rightarrow {}^5/_2$ spin change in Fe(III) porphyrins and heme proteins. For Fe(PPIX)(MeIm)N_3 the reported[37] values are ΔH° = 3.9 kcal mol^{-1} and ΔS° = 11 cal deg^{-1} mol^{-1}. Similar numbers obtain for the azide complexes of met-Mb, met-Hb, and HRP.[38-40] As Table III shows, $\Delta S_k^\ddagger$ for the reaction of MeIm with Fe(TPP)N_3 is 14 eu more positive than that for Fe(TPP)Cl. We suggest that this difference is due to the spin change occurring with the Fe(TPP)N_3 reaction. An alternative explanation would be that $\Delta S_k^\ddagger$ is more positive for Fe(TPP)N_3 relative to Fe(TPP)Cl because the larger azide ion is less strongly solvated in the transition state and so the associated solvent molecules are less ordered. While such an explanation should not be lightly dismissed, we doubt its importance for our reactions because ΔS° for ligand dissociation from FeL^{2+} in aqueous solution is nearly the same for L = N_3^- and Cl^-.[41] We conclude, therefore, that spin-state effects can be large for reactions like eq 1 and can be expected to play a similarly important part in heme protein reactions, e.g. superoxide dissociation from MbO_2 and HbO_2.

The data in Table III can be used to construct the free energy diagrams shown in Figure 9. The energy zero is taken as the reactants Fe(TPP)X + 2RIm. With respect to this energy zero, a number of interesting observations can be made. (1) The transition-state free energy $G^\ddagger$ is *only weakly dependent on the anion* X^-, but depends strongly on the type of nucleophile, MeIm or HIm. Thus $G_{HIm}^\ddagger$ is 3–4 kcal lower than $G_{MeIm}^\ddagger$ reflecting the influence of assisted ionization of X^- via hydrogen bonding to HIm. This causes the activation free energy, $\Delta G_k^\ddagger$, to be about 3 kcal less for the reactions with HIm. A similar lowering of $\Delta G_k^\ddagger$ is observed with Co(TPP)Cl.[30] (2) While hydrogen bonding by HIm lowers $G^\ddagger$ by 3–4 kcal mol^{-1}, the final product, Fe(TPP)(RIm)$_2^+X^-$, is so favored by only 1–2 kcal. (3) The ionization reactions of Fe(TPP)(RIm)N_3 are slower than with the other iron porphyrins because of the lower free energy of Fe(TPP)(RIm)N_3, thus increasing $\Delta G_k^\ddagger$ (but *not* $G^\ddagger$). The low-spin Fe(TPP)(RIm)N_3 complexes must possess substantial CFSE that is lost during the rate-determining conversion to high-spin Fe(TPP)(RIm)$^+N_3^-$. This is no doubt reflected in the much larger $\Delta H_k^\ddagger$ values for Fe(TPP)N_3 relative to those for Fe(Por)Cl (Table III). (4) The rate acceleration produced by HIm is largely an entropic effect. Indeed, the reactions with HIm have a larger $\Delta H_k^\ddagger$ than those with MeIm.

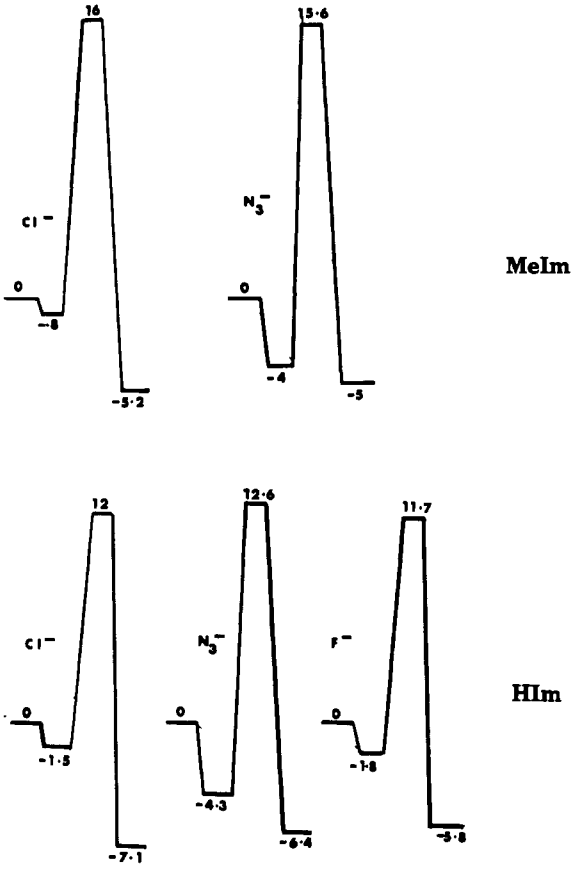

Figure 9. Free energy diagrams for the reaction Fe(TPP)X + 2RIm → Fe(TPP)(RIm)$_2^+X^-$ in acetone at 25 °C. The four energy values shown for each reaction refer to Fe(TPP)X, Fe(TPP)(RIm)X, [Fe(TPP)(RIm)$^+X^-$,RIm]‡ and Fe(TPP)(RIm)$_2^+X^-$. The units are kcal/mol.

Conclusions. This study has shown that hydrogen bonding influences axial ligand ionization in metalloporphyrins and can lower the activation energy by at least several kilocalories per mole. The effect is predominantly entropic, and the magnitude is not markedly dependent on any spin change occurring during the rate-determining step, even though the *absolute* rates depend

(37) Neya, S.; Hada, S.; Funasaki, N.; Umemura, J.; Takenaka, T. *Biochim. Biophys. Acta* **1985**, *827*, 157.
(38) Beetlestone, J.; George, P. *Biochemistry* **1964**, *3*, 707.
(39) Iizuka, T.; Kotani, M. *Biochim. Biophys. Acta* **1969**, *194*, 351.
(40) Tamura, M. *Biochim. Biophys. Acta* **1971**, *243*, 239.
(41) Christensen, J. J.; Eatough, D. J.; Izatt, R. M. *Handbook of Metal Ligand Heats and Related Thermodynamic Quantities*, 2nd ed.; Marcel Dekker: New York, 1975.

strongly on spin changes. The hydrogen-bonding effects seem to be more important in kinetics than in thermodynamics.

Acknowledgment. This work was supported by grants from the National Institutes of Health (Grant Nos. AM 30145 and AM 01151) and the BRSG Fund of Brown University. D.A.S. is the recipient of a NIH Research Career Development Award (1983-1988). J.A.C., A.T.G., E.T.P.K., and T.W. thank their Education and Library boards for undergraduate support grants. J.G.J. thanks Ulster University for a leave of absence.

Contribution from the Department of Chemistry, Washington University, St. Louis, Missouri 63130

A Picosecond Study of Rapid Multistep Radiationless Decay in Manganese(III) Porphyrins

Xinwei Yan, Christine Kirmaier, and Dewey Holten*

Received July 30, 1986

Picosecond transient absorption studies of two Mn(III) porphyrins in coordinating and noncoordinating solvents have revealed two resolvable transient states in each case. The lifetimes of the transients are ≤30 ps and 80 or 140 ps, the faster component being instrument-limited and the slower one depending on the complex. We attribute the transients to the two lowest energy tripmultiplet states that arise from coupling of the ring (π,π^*) triplet and the unpaired metal electrons. The rapid deactivation of both tripmultiplets probably proceeds via lower energy CT or (d,d) excited states.

Introduction

Manganese(III) porphyrins[1] are generally considered to be nonluminescent,[2,3] although a weak ($\phi \sim 10^{-5}$) "phosphorescence" has been reported at low temperature.[4] This essentially nonemissive behavior has been attributed to quenching of the ring (π,π^*) states by lower energy metal ↔ ring charge-transfer (CT) states.[2,3,5-7] Two recent picosecond transient absorption studies have revealed very fast decay of the absorption changes in the 450-600-nm region following photoexcitation, with lifetimes of 17 ps[5] for Mn^{III}TPP(Cl) and 55 ps[6] for Mn^{III}Meso(Cl). These time constants were attributed to radiationless decay of a ring (π,π^*) "tripmultiplet" state. Here we report the results of a picosecond study in which we monitored the absorption changes and kinetics over a more extensive spectral region (500-900 nm). For *both* Mn^{III}TPP(Cl) and Mn^{III}OEP(Cl) in CH_2Cl_2 and in pyridine we observed two transients: one has a fast (≤30 ps) decay and the other a slower relaxation (80 ps for TPP, 140 ps for OEP). We suggest that the short-lived component is the "tripquintet", $^5T_1(\pi,\pi^*)$, a fraction of which relaxes to the longer lived "tripseptet", $^7T_1(\pi,\pi^*)$. Decay of both tripmultiplets probably proceeds via lower energy CT or (d,d) excited states.

Experimental Method

The dual-beam picosecond transient absorption spectrometer used in this work has been described previously.[8] Samples flowing through a 2 mm path length cell at room temperature were excited with a 30-ps flash at either 355 nm (~200 μJ) or 532 nm (up to 1.5 mJ) and probed at various delay times with a 30-ps "white-light" (450-950 nm) pulse. Mn^{III}TPP(Cl) and Mn^{III}OEP(Cl) from Aldrich Chemical Co. were checked by thin-layer chromatography and absorption spectroscopy and were used without further purification. Spectral grade solvents were employed.

Results

Figure 1 shows transient difference spectra from 500 to 640 nm for Mn^{III}OEP(Cl) (A) and Mn^{III}TPP(Cl) (B) in CH_2Cl_2 at two time delays. For both complexes the 7- and 13-ps spectra (acquired during the 30-ps, 355-nm excitation flash) exhibit strong excited-state absorption to the blue of 520 nm, bleaching of the absorption bands in the visible region, and weaker excited-state absorption extending to longer wavelengths. After the excitation flash (67- and 73-ps spectra) much of the strong absorption near 500 nm and a sizable fraction of the bleachings have decayed. Only small, but resolvable, absorption changes remain. Thus, there appear to be two observable transients for each complex; from the 500-640-nm data of Figure 1 the longer lived component is more apparent for the OEP complex than for the TPP complex.

The solid squares in the inset of Figure 2 show that the strong 500-nm absorption for Mn^{III}OEP(Cl) develops and decays essentially with the excitation pulse, placing a time constant of ≤30 ps on the relaxation.[9] The 620-nm absorption of Mn^{III}OEP(Cl) (triangles in Figure 2 inset) clearly decays more slowly, as suggested by the time evolution of the spectra (Figure 1A) and by the data after the excitation flash (and up to 1 ns, not shown); the time constant for the relaxation is 150 ± 30 ps. Mn^{III}TPP(Cl) also exhibits an instrument-limited ≤30-ps decay of the strong absorption near 500 nm, but the residual absorption changes shown in Figure 1B are so small that the kinetics of their disappearance cannot be measured accurately.

In order to measure the decay kinetics of the slower component more accurately, and to search for additional resolvable spectral features, we measured the time evolution of the transient difference spectra between 640 and 900 nm on samples 2-3 times more concentrated than those employed above and excited with stronger flashes at 532 nm. The absorption changes between 640 and 900 nm at 27 ps (solid) and 147 ps (dashed) for both complexes in CH_2Cl_2 are shown in Figure 3. Mn^{III}OEP(Cl) shows a broad transient absorption centered near 690 nm and a trough near 775

(1) Abbreviations used for porphyrin macrocycles: TPP (tetraphenylporphyrin), OEP (octaethylporphyrin), Meso (mesoporphyrin), PPDME (protoporphyrin IX dimethyl ester).
(2) Gouterman, M. In *The Porphyrins*; Dolphin, D., Ed.; Academic: New York, 1978; Vol. III, pp 1-165.
(3) Boucher, L. J. *Coord. Chem. Rev.* **1972**, *7*, 289-329.
(4) (a) Harriman, A.; Porter, G. *J. Chem. Soc., Faraday Trans. 2* **1979**, *75*, 1543-1552. (b) Harriman, A. *J. Chem. Soc., Faraday Trans. 1* **1981**, *77*, 369-377. (c) Becker, R. S.; Allison, J. B. *J. Phys. Chem.* **1963**, *67*, 2662-2669.
(5) Irvine, M. P.; Harrison, R. J.; Strahand, M. A.; Beddard, G. S. *Ber. Bunsen-Ges. Phys. Chem.* **1985**, *89*, 226-232.
(6) Chirvonyi, V. S.; Dzhagarov, B. M. *Fuusika Mat.* **1982**, *31*, 129-132.
(7) Holten, D.; Gouterman, M. In *Optical Properties and Structure of Tetrapyrroles*; Blauer, G., Sund, H., Eds.; de Gruyter: Berlin, 1985; pp 64-90.
(8) Kim, D.-H.; Kirmaier, C.; Holten, D. *Chem. Phys.* **1983**, *75*, 305-322.
(9) Because of possible recycling of molecules that have returned to the ground state during the 30-ps excitation flash, we did not attempt to deconvolute the excited-state decay from the instrument response. We estimate the lifetimes of the short-lived component for both complexes to be 5-30 ps.

0020-1669/86/1325-4774$01.50/0